Multiphysics Analysis of Plasma-Based Tunable Absorber for High Power Microwave Applications

Komlan Payne, *Student Member, IEEE*, Kevin Xu, *Student Member, IEEE*,
Jun H. Choi, *Member, IEEE*, and Jay K. Lee, *Senior Member, IEEE*

***Abstract*— Power handling capability of a tunable plasma-based multilayer absorber is studied using multiphysics analysis, then validated by experimental data. The proposed two-pole absorber is based on conductor-backed thickness customizable high-order bandpass frequency selective surfaces (FSSs). Such technique allows simple integration of the tuning elements, while simultaneously providing the option to realize FSSs (including absorbers) with specific/desired thicknesses and transfer responses. Lossy magneto-dielectric slabs, used to absorb electromagnetic energy in the C-band, are added between the metallic layers. The lossy slabs are perforated to host discrete, electrically tunable, ceramic gas-encapsulating chambers (plasma-shells), enabling dynamic control of the absorption spectral band. To study the power handling capability of the proposed multi-layered tunable absorber, dielectric and air breakdowns within the device are numerically emulated using EM simulation by quantifying the maximum field enhancement factor (MFEF). Furthermore, a comprehensive thermal analysis using a simulation method that couples electromagnetics and heat transfer is performed for the absorber under high power continuous microwave excitations. Since heat generated within the absorber is a primary concern, the steady state as well as transient state temperature distributions have been evaluated for various incident power densities. The performance of the proposed absorber is validated for a prototype having a finite size of 13×13 cm^2.**

***Index Terms*— Active high impedance surface, circuit analog absorber, electromagnetic interference, electromagnetic pulse, high power microwave, lossy frequency selective surfaces, radar cross section, RF plasma discharge, tunable absorber.**

I. Introduction

MULTIPHYSICS analysis is a powerful design process that can be used to understand multiple physical phenomena of electromagnetic devices under real world conditions. Such analysis, composed of electromagnetic (EM) simulation coupled with thermal, structural, and/or fluidic simulations [1], [2] are critical for the design liability associated with performance and cost. One of the real-world applications of multiphysics analysis involves the impact of high-power electromagnetic interference (EMI) with electronic devices. In such events, researchers have focused their understanding on electronic attacks (EA) and electronic protection (EP). These inquiries have led to tremendous development capabilities that are evolving rapidly with modern technology [3]–[5]. Advanced countermeasures electronic systems, such as electronic coating shielding, isolators, filter limiters, frequency selective surfaces, microwave absorbers [6]–[14], etc., have been explored to ensure functional safety of EM devices. Conversely, techniques such as electronic jamming and deception, anti-radiation weapons, use of high-power microwave (HPM) and electromagnetic pulse (EMP) weapons [15]–[21] are often exploited to target those protective layers and damage the electronic and electric systems through EM coupling. The exposure of electronic systems to high power level EM interference, whether it is intentional or not, can disrupt their performance and cause device failure depending on the core material and the microscopic features of the systems architecture. Usually, the electric fields induced in the system caused by the incident wave are associated with current and voltage surges that can initiate electromagnetic breakdown, arcing or overheating of the system [22]. Under such conditions, design specifications such as EM-thermal-mechanical management can no longer be neglected. The ANSYS multiphysics simulator has proven to be a reliable and powerful software package for the study of EM-thermal-mechanical coupling [23], [24]. While the EM analysis is performed by ANSYS HFSS, both thermal analysis and stress analysis can be performed using ANSYS Mechanical. For instance, if the electronic system is lossy, the electric fields calculated from Maxwell's equations are used to compute the power dissipated in the system. The EM losses (surface and volume loss densities) are then converted into heat using heat transfer equations. Then, the temperature distribution can be utilized to analyze the thermal stress (expansion or contraction). The deformation caused by the thermal stresses and the change in temperature are fed back into HFSS and will affect the electro-thermal properties of the materials. This cycle is repeated until the temperature reaches its steady state. The interaction between EM and heat transfer using both ANSYS HFSS and ANSYS Mechanical provides an accurate and complete bidirectionally coupled physics analysis. In this paper, the physical limitation of a plasma-based tunable conductor-backed absorber under high power microwave levels is

Manuscript received September 15, 2020; revised January 26, 2021; accepted March 22, 2021. This work is supported by the Air Force Office of Scientific Research under AFOSR Award FA9550-17-1-0111 and in part by the National Science Foundation under NSF award ECCS-1908546. This work is also supported in part by Syracuse University through computational resources. *(Corresponding author: Komlan Payne.)*

K. Payne and J. K. Lee are with the Department of Electrical Engineering and Computer Science, Syracuse University, Syracuse, NY 13244 USA (e-mail: kopayne@syr.edu; leejk@syr.edu).

K. Xu and J. H. Choi are with the Department of Electrical Engineering, University at Buffalo, Buffalo, NY 14260 USA (e-mail: kxu22@buffalo.edu; junhchoi@buffalo.edu).

This article has been accepted for publication in a future issue of this journal, but has not been fully edited. Content may change prior to final publication. Citation information: DOI 10.1109/TAP.2021.3070088, IEEE Transactions on Antennas and Propagation

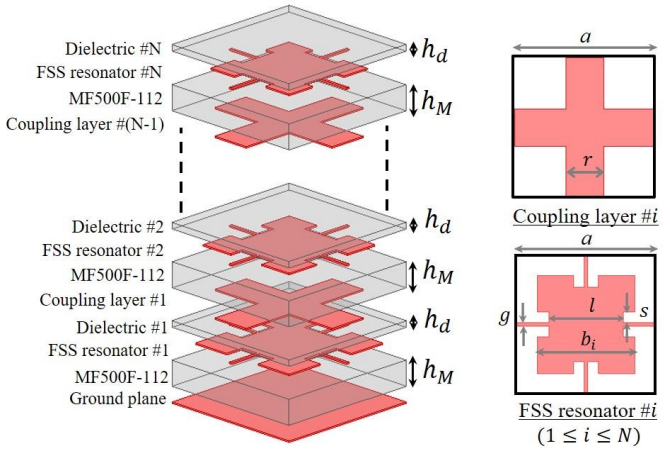

Fig. 1. Topology of the multipole/high-order ($N \geq 2$) absorber unit cell based on coupling interlayers along with detailed geometry of each layer.

TABLE I. PHYSICAL DIMENSIONS (IN MM) AND ELECTRICAL THICKNESS OF VARIOUS HIGH-ORDER ABSORBERS.

Design	Size	h_M	h_d	a	g	s	l	r	b_1	b_2	b_3
2^{nd} *order*	$\lambda_0/7$	3	0.8	12.5	0.30	1.5	6.5	3.9	9.3	8.2	--
3^{rd} *order*	$\lambda_0/4$	3	0.8	12.5	0.15	1.6	6.5	4.0	9.2	9	7.8

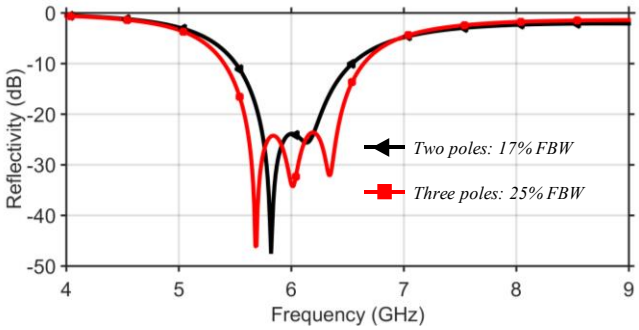

Fig. 2. Simulated reflection coefficient of the multipole absorbers with second and third order response.

demonstrated using multiphysics numerical analysis.

In general, most microwave absorbers are backed by a perfect conductor acting as a ground plane. These artificial surfaces prevent RF interference from impacting sensitive electronics used for military and aerospace applications [25]. The ultimate goal of absorber is to minimize the probability of detection or provide environment sealing of microwave systems by preventing reflection through absorption of the EM wave due to their structural lossy materials [26]. The working principle of conventional multilayer conductor-backed absorbers, such as Jaumann [27] and Dallenbach [28] absorbers, is circumscribed to the quarter-wavelength resonator concept. In Jaumann absorbers, the incident electromagnetic energy is dissipated within lossy homogeneous sheets, while Dallenbach absorbers are contingent on the dielectric and magnetic losses of the stacked substrates. With the evolution of FSS designs, new radar absorbers including circuit analog absorbers (CAAs) [25], [29] and "metamaterial absorbers" [30]–[32] have been introduced. CAAs use cascaded lossy bandstop FSS sheets about quarter-wavelength apart between layers, similar to the Jaumann absorber, but with broadband performance. On the other hand, "metamaterial absorbers" or FSS-based absorbers exhibit a controllable design thickness. The absorption band for such an arrangement is predominantly determined by the operating frequency of the constituent reactive elements that comprise the FSS, and the loss in the design is introduced using either resistive FSS sheets or lossy substrates [33]. They provide artificial boundaries to the electromagnetic waves and can be used to implement either very thin narrowband absorbers or thick wideband absorbers. However, the physical bound imposed on the thickness-to-bandwidth ratio (also known as Rozanov limit) carries a crucial limitation on passive absorbers [34]. To circumvent the aforementioned tradeoff, reconfigurable absorbers can be designed to mitigate the RCS of prospective targets from frequency agile radar tracking interrogation signals.

Besides the use of plasma-based reconfigurable microwave components, other tuning components include PIN diodes, semiconductor and ferroelectric varactors, liquid-crystal polymers, and graphene [35]–[41]. However, the current mainstream tuning components compromise the design performance factors such as tuning range, reliability, linearity, cost, and weight. For instance, plasma and graphene are better suited to assure stable operation when exposed to high power EM radiation. The advantage of using discrete plasma-shells over some existing tuning components for reconfigurable devices has been addressed in [12]–[14]. The tuning mechanism of these discrete plasma-shells is already fully analysed in [14] using their equivalent circuit model. In [12], by selecting core materials for higher temperature operation, absorbers that incorporate lossy substrates are suitable for HPM energy. In contrast, the absorbers that utilize resistive sheets made of thin-film nickel phosphorous, nickel chromium, nickel chromium aluminum silicon, or chromium silicon monoxide (foils available on Rogers substrates from Ticer and Ohmega Technologies) operate in relatively lower temperature ranges but provide superior absorption bandwidth because of their frequency-independent electrical properties over a broader frequency range. By leaning toward applications requiring protection from high power microwave/electromagnetic pulse (HPM/EMP) emanated by frequency agile microwave weapons or radar systems, we introduced a multilayer absorber [42] comprised of FSS layers, and a rigid magnetically loaded high temperature material (with an operable temperature up to 260°C). The commercially available lossy magneto-dielectric Eccosorb MF500F series materials from Laird are used to absorb the electromagnetic energy. The proposed absorber, shown in Fig. 1, adopts the design technique for thickness customizable high-order ($N \geq 2$) bandpass FSSs [43] placed above a ground plane to realize a compressed Dallenbach type of absorber. Then reconfigurability and independent control of each resonant frequency is added to the multipole design by incorporating discrete plasma-shells into the lossy magneto-dielectrics. Rectangular cavities are milled out of the lossy substrates to precisely fit the dimensions of the shells.

This article has been accepted for publication in a future issue of this journal, but has not been fully edited. Content may change prior to final publication. Citation information: DOI 10.1109/TAP.2021.3070088, IEEE Transactions on Antennas and Propagation

TABLE II. PHYSICAL DIMENSIONS (IN MM), ELECTRICAL THICKNESS AND FBW OF THE THREE DESIGN CONFIGURATIONS WITH SECOND ORDER RESPONSE ($N = 2$).

Design	*Size*	h_M	h_d	a	g	s	l	r	b_1	b_2	*FBW*
#1	$\lambda_0/9$	2	0.8	12.5	0.17	1.56	6.5	3.6	9.3	8.3	17%
#2	$\lambda_0/7$	3	0.8	12.5	0.30	1.50	6.5	3.9	9.3	8.2	17%
#3	$\lambda_0/5$	4	0.8	12.5	0.35	1.47	6.5	4.2	9.3	8.2	17%

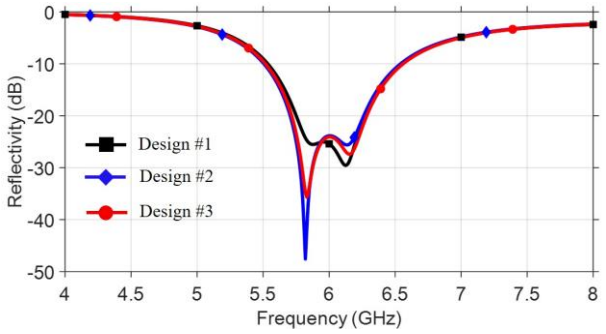

Fig. 3. Simulated reflection coefficient of the three passive absorber configurations (without plasma-shells) using different thicknesses.

The work presented in this paper covers two segments. First, a full-wave electromagnetic simulation is carried out to validate the performance of the proposed absorber operating in the C-band at OFF state under various angles of incident wave. In order to emulate its reconfigurability, the plasma frequencies are adjusted accordingly to tune the surface impedance of each resonator. A finite size prototype is fabricated using photolithography process. Under free space measurement, the absorptivity and tuning capability of the device are obtained and compared with numerical results. In the second segment, the peak power (for very short duration pulse) and average microwave power (for continuous wave) handling capability of the active absorber is been investigated. A numerical analysis is carried out to predict the dielectric and air breakdown levels within the system. Also, since the absorber converts the EM energy into thermal energy, the EM wave and heat transfer are coupled together to evaluate the thermal behavior of the absorber. Both the steady state and transient state analysis are performed when the device is exposed to various incident power densities. A non-uniform temperature distribution is obtained with hotter spot located within the lossy magneto-dielectric. Since testing at high power microwave levels is potentially unsafe, experiments are performed with relatively moderate far-field power densities to validate numerical results. The temperature distributions on the top surface of the absorber are obtained using a thermal imaging infrared camera (FLIR E6).

II. DESIGN PROCEDURE OF THE PROPOSED MULTILAYER PLASMA-BASED TUNABLE ABSORBER

A. Design implementation and simulation results

The proposed N^{th} order multipole absorber, illustrated in Fig. 1, comprises the ground plane along with a high-order ($N \geq 2$) bandpass FSS containing N metallic bandpass FSS

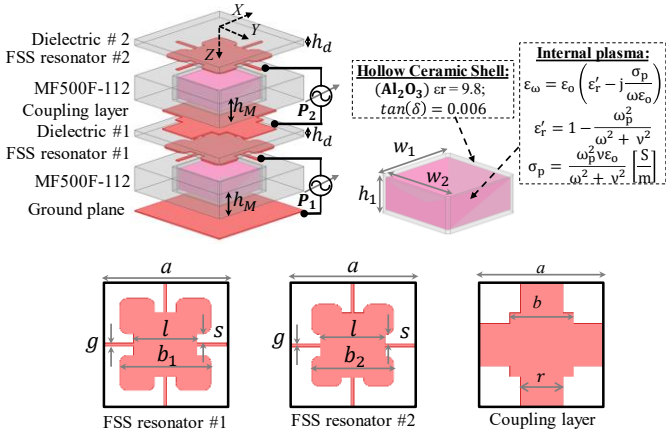

Fig. 4. Two-pole tunable plasma-based absorber unit cell based on coupling interlayers with plasma-shells ($h_M = 3.5$ mm, $h_d = 1.524$ mm, $a = 10$ mm, $g = 0.4$ mm, $s = 1.65$ mm, $b_1 = 9.4$ mm, $b_2 = 8.66$ mm, $l = 6.5$ mm, $b = 6.5$ mm, $r = 3.6$ mm, $w_1 = w_2 = 6$ mm, and $h_1 = 3.3$ mm).

resonators, N lossy substrates, N dielectrics slabs and (N-1) metallic coupling interlayers. The FSS is formed by a two-dimensional array of miniaturized resonators that behave as a parallel LC bandpass filter to the EM wave incident to the FSS surface. The lossy substrates, made of Eccosorb MF500F-112 sheets with thickness h_M, are used to dissipate the EM energy. The mesh grid metallic interlayers are placed between resonator layers to regulate their coupling level for any given separation. Such degree of design freedom provided by the coupling interlayers brings practical benefits when utilizing standard commercial substrate thicknesses and integrating tuning elements that require precise control of physical dimensions. The metallic resonator and coupling layers are etched from Rogers RO4003C laminates with thickness h_d, which are chosen as the dielectric layers for their thermal stability. A second ($N = 2$) and third ($N = 3$) order response are implemented to obtain absorption in the C-band (4 GHz to 8 GHz). The lossy MF500F-112 slabs are accurately modeled in HFSS using their specified frequency-dependent electric and magnetic properties (real part of permittivity and permeability, electric loss tangent, and magnetic loss tangent). The physical dimensions of the various high-order absorbers are summarized in Table I. The simulated full wave EM results illustrated in Fig. 2 predict absorption of the EM wave in the C-band centered at 6 GHz with 17% and 25% fractional bandwidth (FBW) at 10 dB reflectivity level for the second and third order absorbers, respectively. The total thickness of the two-pole absorber is 8 mm (about $\lambda_0/7$) and the periodicity in the order of $0.25\lambda_0$, where λ_0 is the free space wavelength at 6 GHz. For the three-pole absorber the total thickness is 12 mm (about $\lambda_0/4$) with the periodicity in the order of $0.25\lambda_0$.

To demonstrate the design flexibility in accommodating different material thicknesses, the two-pole absorption response (17% FBW at 10 dB reflectivity level) is obtained using three different MF500F-112 thicknesses ($h_M = 2$ mm, 3 mm, and 4 mm). The physical dimensions (in mm) of the absorber for each configuration are summarized in Table II. The results obtained in Fig. 3 show that the absorber can be scaled to different thicknesses while preserving the same absorption characteristic (center frequency and fractional bandwidth).

This article has been accepted for publication in a future issue of this journal, but has not been fully edited. Content may change prior to final publication. Citation information: DOI 10.1109/TAP.2021.3070088, IEEE Transactions on Antennas and Propagation

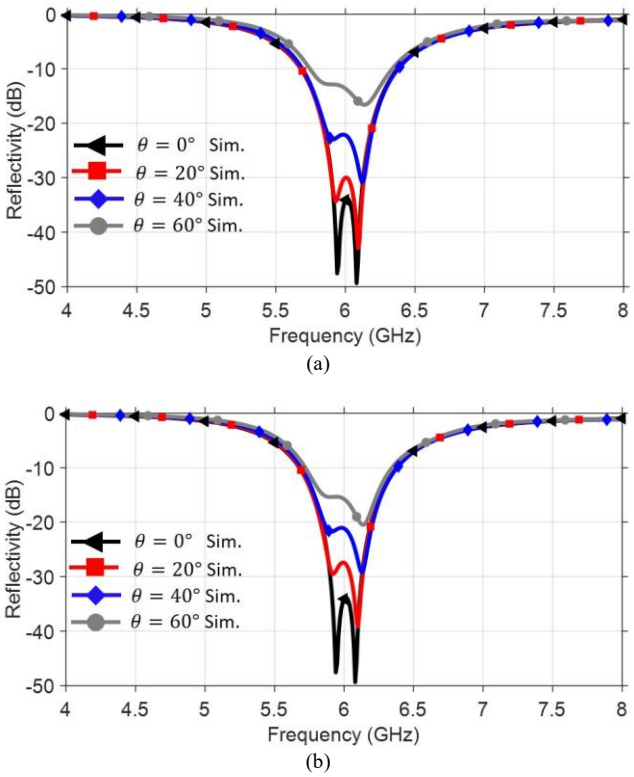

Fig. 5. Full wave simulated reflection coefficient of the multilayer absorber at OFF state for various oblique angles of incident wave. (a) TE polarization. (b) TM polarization.

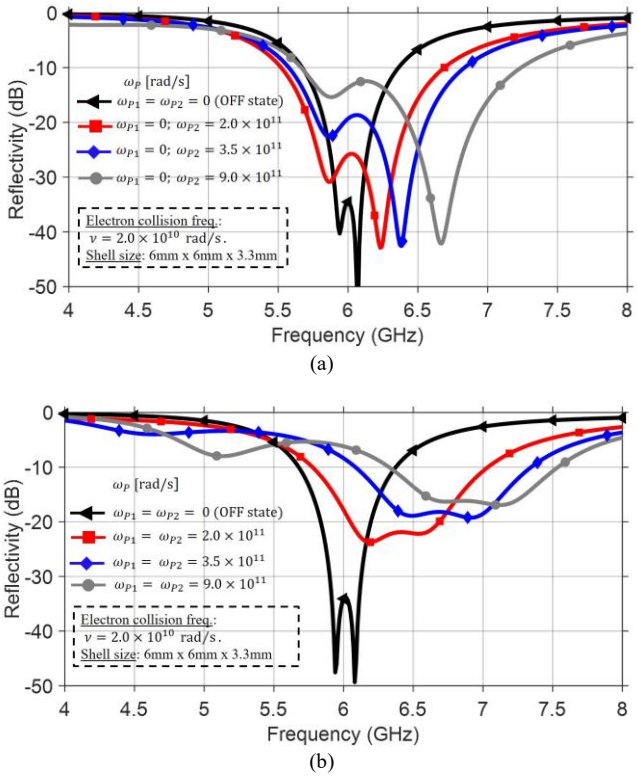

Fig. 6. Full wave simulated reflection coefficient of the multilayer absorber at ON state subject to different plasma frequencies. (a) Only the top plasma layer is activated and (b) Both plasma layers are activated.

In order to add the reconfigurability feature to the two-pole absorber, hollow ceramic gas-encapsulating chambers (plasma-shells) are embedded in the lossy magneto-dielectric layers sandwiched between metallic layers as shown in Fig. 4. The edges of the resonator patches are rounded with a fillet radius of 0.7 mm to minimize field enhancement at the sharp corners. In the proposed design, both the resonators and the coupling interlayers are used as biasing surfaces for the shells (*shell size*: 6 mm × 6 mm × 3.3 mm). The shells are made of alumina (Al_2O_3) using a wall thickness of 0.2 mm. Silver epoxy of 0.1 mm thickness (not shown in the figure) is inserted between the shells and metallic layers to ensure electrical contact to the shell. The cold collisional plasma volume is modeled as a complex frequency and electron density dependent material with permittivity ε_p expressed as follows [44]:

$$\varepsilon_p = \varepsilon_0(\varepsilon_r^{'} - j\frac{\sigma_p}{\omega\varepsilon_0}) \tag{1}$$

where $\varepsilon_0 = 8.854\times10^{-12}$ F/m is the permittivity of free-space, $\varepsilon_r^{'}$ is the real part of relative permittivity, σ_P [S/m] is the conductivity and ω [rad/s] is the angular operating frequency.

$$\varepsilon_r^{'} = 1-\frac{\omega_p^2}{\omega^2+\nu^2};\ \sigma_p = \frac{\omega_p^2\nu\varepsilon_0}{\omega^2+\nu^2}\left[\frac{S}{m}\right];\ and\ \omega_p \approx 56.4\sqrt{n_e} \tag{2}$$

where ω_p [rad/s], ν [rad/s], and n_e [m^{-3}] are plasma frequency, electron collision frequency, and electron density, respectively. The physical dimensions of the active absorber using commercially available thicknesses of RO4003C and MF500F-112 are depicted in the caption of Fig. 4. Simulation results at OFF state ($\omega_{p1} = \omega_{p2} = 0$) shown in Fig. 5 predict a stable absorption response across the absorption band for both transverse electric (TE) and transverse magnetic (TM) polarizations when the system is illuminated from various oblique incident angles ($0° \le \theta \le 60°$). However, above 40° angle of incidence, the reflectivity of the absorber has increased to above −20 dB.

The variation of the biasing voltage is mimicked by applying different plasma frequencies through simulation. The electron collision frequency of the plasma is set to its optimal value $\nu = 2.0 \times 10^{10}$ rad/s. On one hand, we assume that only the top plasma layer is excited ($\omega_{p1} = 0$). The variation of the plasma frequency ($0 \le \omega_{p2} \le 9 \times 10^{11}$ rad/s) predicts a tuning of the absorption spectrum and rate. The higher absorption resonant frequency has shifted from 6.2 GHz to 6.7 GHz (see Fig. 6(a)). However, a wider absorption band is obtained at the expense of the absorption rate. On the other hand, when both plasma layers are excited, the effect of the variation of the plasma frequencies such that $\omega_{p1} = \omega_{p2}$ (see Fig. 6(b)) predicts a tuning of both resonant frequencies across the C-band. Consequently, the center frequency shifts to higher value (from 6 GHz to 7 GHz).

B. Fabrication processes and measurement results

The proposed multilayer plasma-based tunable absorber is fabricated and tested in a free space environment to validate the numerical results. The metallic resonators and coupling layer are patterned on the RO4003C substrates using wet etching

This article has been accepted for publication in a future issue of this journal, but has not been fully edited. Content may change prior to final publication. Citation information: DOI 10.1109/TAP.2021.3070088, IEEE Transactions on Antennas and Propagation

Fig. 7. Fabricated perforated lossy magneto-dielectric (MF500F-112).

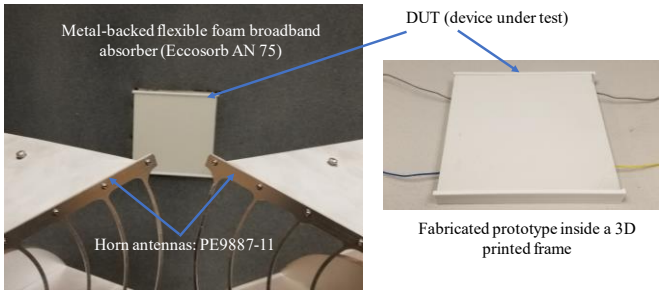

Fig. 8. Photograph of the test setup (free space) along with the fabricated prototype inside a 3D printed frame.

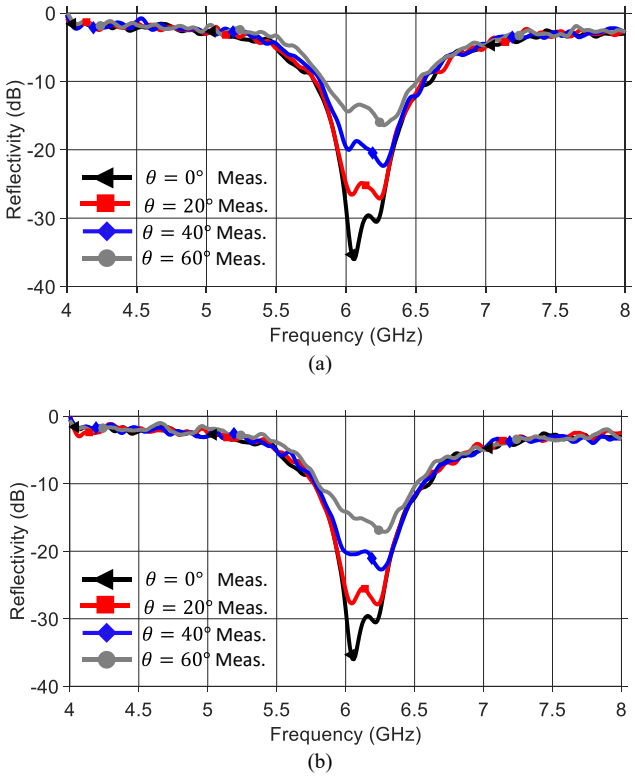

Fig. 9. Measured reflection coefficient of the multilayer absorber at OFF state for various oblique angles of incident wave. (a) TE polarization. (b) TM polarization.

process. Also, the magneto-dielectric substrates MF500F-112 are finely drilled and perforated using a milling machine (LPKF ProtoMat S103) as shown in Fig. 7. The prototype board is an array of 13 × 13 elements, printed on the RO4003C substrates with a total size of 130 mm × 130 mm. The plasma-shells, manufactured by Imaging Systems Technology Inc., are filled with a 0.1 % Argon - 99.9 % Neon mixture at 100 Torr gas pressure. The electron collision frequency ($\nu = 2.0 \times 10^{10}$ rad/s) was used to estimate the required gas pressure at 300 K electron temperature (T_e) by solving the theoretical expression for neon gas derived in [45]:

$$\nu[\mathrm{s}^{-1}] = 8.63\times10^{-18} \times \left(\frac{P}{K_B T_e}\right) \times T_e^{0.833} \quad for \quad 10^2 K \le T_e \le 5\times10^3 K \tag{3}$$

where K_B [J.K^{-1}] is Boltzmann's constant, and P [Pa] is gas pressure. The fabrication procedure of the multilayer absorber with the plasma-shells embedded in the lossy perforated magneto-dielectric substrates MF500F-112 is as follows: (a) the shells are hand-placed in the perforated lossy magneto-dielectric (MF500F-112) backed by the ground conductor; (b) conductive silver epoxy is deposited on the top side of the shells using a syringe; (c) the bottom plasma excitation layer is added on top of the lossy magneto-dielectric; (d) the second perforated lossy magneto-dielectric is added on top of the bottom plasma excitation layer; (e) shells with epoxy deposited on both top and bottom side are hand-placed in the substrate chambers; (f) the top plasma excitation layer is added on top of the magneto-dielectric. A frame made of thermoplastic material using a 3D printer (Monoprice Maker Select v2) is used for precise alignment and to hold the layers together. The device under test (DUT) is then mounted at the center of a commercially available large metal-backed foam broadband absorber (Eccosorb AN-75), where an aperture is cut out to fit the DUT dimensions, as shown in Fig. 8. The Eccosorb AN-75 frame is used to reduce edge diffraction effects of the finite sized DUT. The calibration procedure is the same as previously described in [14]. The reflection coefficient of the absorber is characterized at OFF state across incident angles up to 60° for both TE and TM polarizations. The measured results (Fig. 9) show stable reflection response when the system is illuminated from oblique angles of incidence, and acceptable agreement with the simulated results (Fig. 5) is demonstrated, although the measured center frequency has shifted slightly to 6.1 GHz.

In order to turn the device ON, a class A, RF power amplifier (ENI 2100L with 50 dB nominal gain and operating frequency ranging from 10 KHz to 12 MHz) is used to sustain the plasma layers. The RF power amplifier (PA) amplifies a 2 GHz sinusoidal wave generated from a Keysight N5181A MXG RF analog signal generator. The output of the PA is then connected to the bias traces of the absorber via a coaxial cable. By monitoring the power level of the continuous wave through the PA front panel meter and changing the voltage from the signal generator, different voltage is supplied to the plasma volume. The tuning speed observed is less than 100 ns. The excited device under test is shown in Fig. 10. When only the top plasma layer is excited with various RF power such that $P_1 = 0$ and $0 \le$

This article has been accepted for publication in a future issue of this journal, but has not been fully edited. Content may change prior to final publication. Citation information: DOI 10.1109/TAP.2021.3070088, IEEE Transactions on Antennas and Propagation

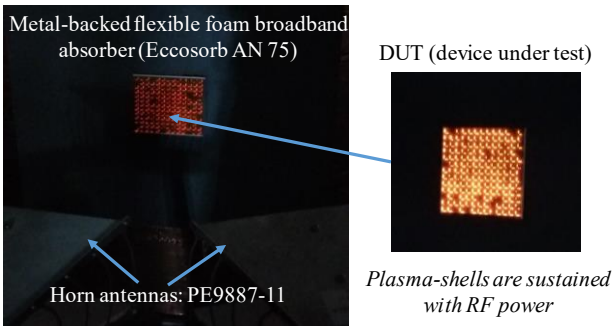

Fig. 10. Photograph of the test setup (free space) of the absorber when the plasma is sustained with RF power.

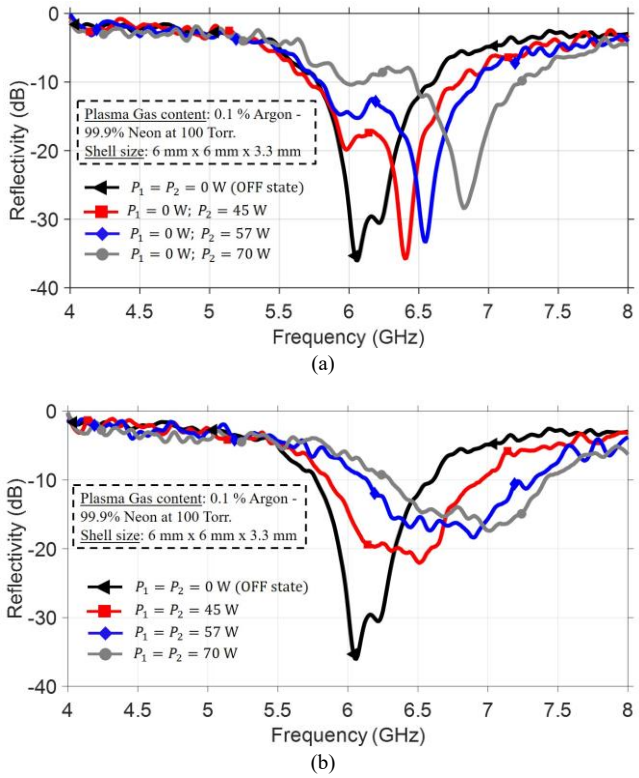

Fig. 11. Measured reflection coefficient of the multilayer absorber at ON state. The plasma volume is excited independently excited with various RF power intensities. Tuning capability observed for (a) Only the top plasma layer is activated and (b) both plasma layers are activated.

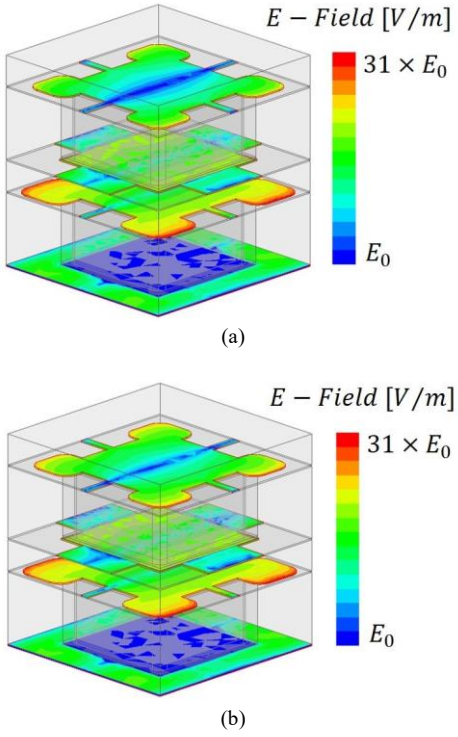

Fig. 12. Simulated E-field distribution in the metallic layers at a unit cell level of the absorber illuminated with an incident power of 1 W. The electric field with intensity $E_0 = 2746$ V/m is coupled to the absorber. The induced field distribution is observed at (a) the first resonant frequency $f_1 = 5.9$ GHz; (b) the second resonant frequency $f_2 = 6.1$ GHz.

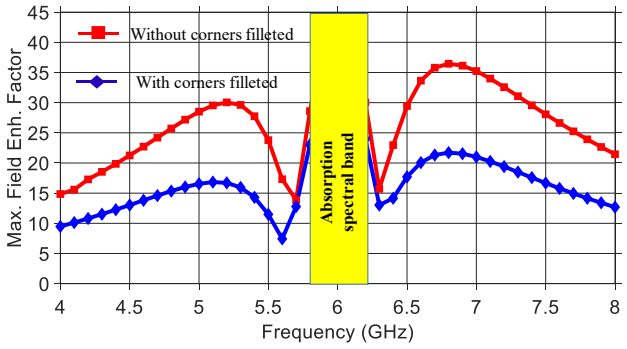

Fig. 13. Extracted MFEF values at different frequencies of the absorber without and with filleted resonator corners.

$P_2 \leq 70$ W, the measured results at normal angle of incidence indicate a tuning of the higher absorption resonant frequency (see Fig. 11(a)). However, when both plasma layers are activated ($0 \leq P_1 = P_2 \leq 70$ W), a tuning of the absorption spectrum range is perceived (see Fig. 11(b)) showing a shift of the absorption center frequency. The measured results obtained in Fig. 11 agree well with their simulated results shown in Fig. 6. These experimental results validate the fact that the proposed absorber, when properly biased, can be adapted under a dynamic EM environment.

III. Physical Impact of High-Power Microwave Source on the Proposed Multilayer Absorber

High peak and average microwave power sources present severe challenges for the reliability and safety of resonant structures. Under exposure of high-power RF, the physical interaction between the EM field and the electronic system on a molecular level must be investigated. Electromagnetic breakdown and overheating of the device are feasible causes of design failure. In general, EM breakdown events are the primary concerns associated with very short pulse durations (in

This article has been accepted for publication in a future issue of this journal, but has not been fully edited. Content may change prior to final publication. Citation information: DOI 10.1109/TAP.2021.3070088, IEEE Transactions on Antennas and Propagation

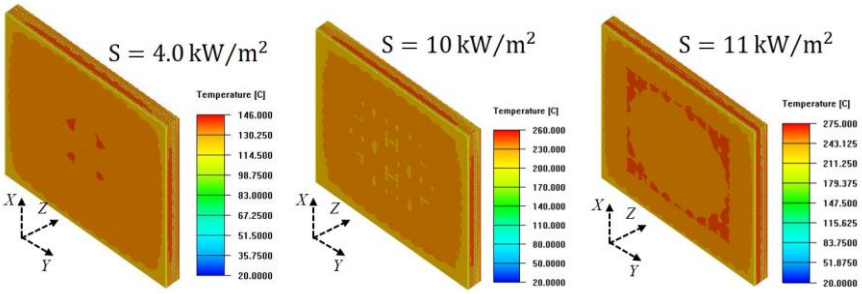

Fig. 14. Simulated steady state temperature map throughout the multilayer absorber exposed to various power densities with incident plane wave at f_0 = 6 GHz.

TABLE III. APPROXIMATED MAXIMUM ALLOWED POWER DENSITY $(in\ MW/m^2)$ FOR VERY SHORT PULSE DURATION OF HIGH POWER

Design	5.8 GHz	5.9 GHz	6 GHz	6.1 GHz	6.2 GHz
Without filleted resonator corners	14.5	7.2	10.4	7.5	13.2
With filleted resonator corners	22.5	12.3	14.2	12.5	20.7

TABLE IV. THERMAL PROPERTIES OF THE ABSORBER MATERIALS

Material	Thermal conductivity ($W.m^{-1}.K^{-1}$)	Density ($Kg.m^{-3}$)	Specific heat ($J.Kg^{-1}.K^{-1}$)	Operating temperature limit (ºC)
Copper	401	8933	356	< 750
Alumina	27	3970	910	< 1750
Neon	0.0498	0.1079	1029.9	< 1000
RO4003C	0.71	1700	900	< 280
MF500F	1.44	3250	1300	< 260

terms of μs) of high peak power. This happens when the induced electric field within the device becomes greater than the breakdown limit of air or the dielectric. In our resonant absorber, the slots within the metallic layers enhance the localized electric field intensity from a buildup of negative and positive charges. As a result of the electric discharge, current will flow through the dielectric to create a short circuit as the insulating material becomes a good conductor. On the other hand, overheating of the system is associated with high average power with sustained continuous wave. The energy dissipated in the system due to the time-averaged metallic and dielectric losses is converted into heat, which can become problematic depending on the selected design materials.

A. Estimation of the absorber breakdown threshold

The prediction of the absorber electrical breakdown level is a very complex task because the discharge process is transient and occurs on a microscopic level. The commercial EM tool Spark3D coupled with the high-performance 3D EM analysis software CST has proven to be a more sophisticated tool for determining RF breakdown power level within microwave devices. The interface of such EM tool provides a real-time 3D view of the electric discharge at the localized region. While cutting-edge methods are used by Spark3D to predict microwave breakdown discharge, we exploit the effect of the field enhancement caused by high peak microwave power in a simple fashion. The ratio of the maximum electric field intensity to the incident electric field intensity, known as the maximum field enhancement factor (MFEF) [46], can be calculated to estimate the power handling capability of the design relative to other periodic structures. A lower MFEF indicates lower risk of reaching air and dielectric breakdown levels within the absorber and therefore better resiliency toward high power EM waves is expected. However, at resonance the fields inside small metallic gaps are maximally enhanced. For example, an incident power of 1 W illuminating the proposed unit cell (with periodicity a = 10 mm) corresponds to an incident power density of 10,000 W/m^2 and incident electric field intensity of E_0 = 2746 V/m. The electric field distribution in the metallic layers of the absorber unit cell at both resonance frequencies (f_1 = 5.9 GHz and f_2 = 6.1 GHz), obtained using HFSS, is shown in Fig. 12. Strong local field enhancement is observed at the edges of both metallic FSS resonators. The MFEF, plotted in Fig. 13, is extracted across the C-band (4 GHz to 8 GHz) for the absorber with and without filleted resonator corners. It is perceived that the proposed design with filleted resonator corners shows slightly better performance in handling higher microwave power levels. The MFEF is found to be greater in the operating band of the absorber, with maximum value (MFEF ≈ 31) obtained at both resonant frequencies for the proposed design. At OFF state, the air gap existing in the metallic slots is the most limiting medium, with electrical breakdown occurring at E_B = 3 MV/m. For a very short pulse duration of high peak power, the maximal power density the absorber can withstand at specific frequencies is depicted in Table III. Overall, the data obtained shows the maximum allowed incident power density is about S = 12.3 MW/m^2 for the proposed multilayer absorber at OFF state.

B. Thermal analysis of the proposed multilayer absorber

As mentioned previously, when the absorber is coupled with a high average power continuous wave (CW), thermal analysis needs to be taken into account to avoid design failure due to material heating and possible burning. Therefore, it is important

This article has been accepted for publication in a future issue of this journal, but has not been fully edited. Content may change prior to final publication. Citation information: DOI 10.1109/TAP.2021.3070088, IEEE Transactions on Antennas and Propagation

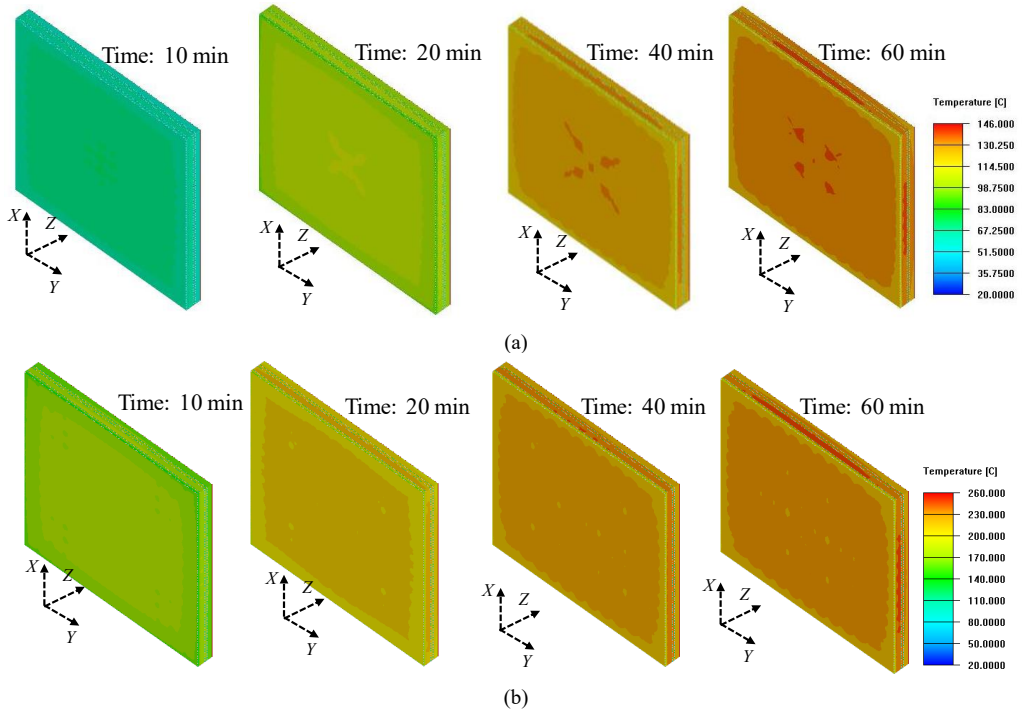

Fig. 15. Simulated transient state temperature map throughout the multilayer absorber with incident plane EM wave at f_0 = 6 GHz. The absorber is exposed to various power densities. (a) S = 4.0 kW/m^2; (b) S = 10 kW/m^2.

TABLE V. SIMULATED MAXIMUM TEMPERATURE (°C) WITHIN THE MF500F SUBSTATES FOR DIFFERENT POWER DENSITIES ACROSS THE ABSORPTION SPECTRAL BAND

Power Density	5.8 GHz	5.9 GHz	6 GHz	6.1 GHz	6.2 GHz
S = 1.0 kW/m^2	60.5	62.7	60	61.5	61
S = 4.0 kW/m^2	145	146.7	146	146.9	146
S = 10 kW/m^2	261	259.5	260	261	260.5
S = 11 kW/m^2	275.4	274.8	275	275	274.6

TABLE VI. FOUR DIFFERENT TUNING STATES OF THE PLASMA ALONG WITH THEIR RESPECTIVE PLASMA FREQUENCIES AND ABSORPTION CENTER FREQUENCIES.

Tuning state	Plasma frequency	Sim. center frequency	Meas. center frequency
OFF State	0	6.0 GHz	6.1 GHz
ON State #1	2.0 × 10^{11} rad/s	6.4 GHz	6.3 GHz
ON State #2	3.5 × 10^{11} rad/s	6.7 GHz	6.7 GHz
ON State #3	9.0 × 10^{11} rad/s	6.9 GHz	6.9 GHz

to understand how the material choice can affect the thermal and electrical performance of the design. The CW incident power density allowed by the design can be obtained based on the thermal limit of their temperature dependent materials. A comprehensive multiphysics solution that couples full-wave EM to thermal analysis is performed using HFSS and Icepak from ANSYS. In general, the temperature dependency of the materials' electrical properties (such as dielectric constant, loss tangent, conductivity) are governed using a quadratic approximated equation [47]:

$$x(T) = x(T_0)\left[1 + C_1\left(T - T_0\right) + C_2\left(T - T_0\right)^2\right] \quad (4)$$

where T_0 is the initial temperature, T is the temperature of the heated material (which can be position dependent as well), and C_1 and C_2 are the linear and quadratic expansion coefficients, respectively. A bidirectionally coupled analysis is possible if the temperature dependency of all the materials' electrical properties is known. In such case, the transient frequency response of the design due to temperature drift and structural deformation can be also obtained. However, in this section our analysis focuses on the heat generated solely due to Joule heating within the absorber for different incident power densities. The thermal specification of the design modeled in Icepak is illustrated in Table IV. These values are taken under ordinary conditions and it can be seen that the magneto-dielectric MF500F-112 is the limiting material in terms of the maximum operating temperature (< 260 ºC). Beyond this maximum operating temperature (MOT), the hard polymer loses its electrical and mechanical integrity. The simulation setup in Icepak is performed in a natural convection environment (heat transfer coefficient HTC = 10 W.K^{-1}.m^{-2}), with the radiation ON (for heat transfer) and ambient external temperature. In order to predict the temperature profile of the design, the exact finite size of the absorber is taken into account to consider the edge effects, although a heavy simulation CPU time is required. Both the steady and transient state simulation results are obtained when the absorber is exposed to a continuous plane wave. The steady state temperature profile of the absorber exposed to various power densities at the center

This article has been accepted for publication in a future issue of this journal, but has not been fully edited. Content may change prior to final publication. Citation information: DOI 10.1109/TAP.2021.3070088, IEEE Transactions on Antennas and Propagation

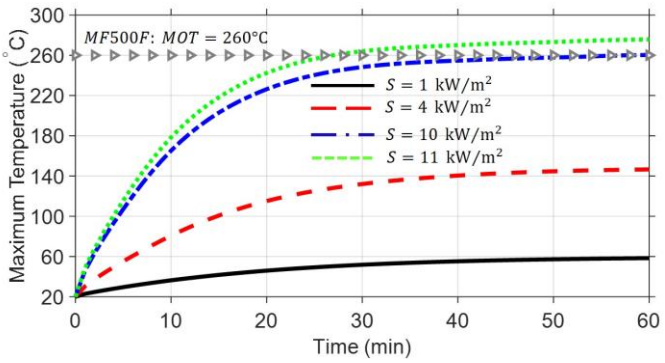

Fig. 16. Time-variant simulated peak temperature plot at OFF state throughout the MF500F substrates illustrated for various power densities with incident plane EM wave at f_0 = 6 GHz.

frequency (f_0 =6GHz) is illustrated in Fig. 14 (which reflect the temperature plot in both substrates and metallic surfaces). It appears that a non-uniform spatial temperature distribution is obtained such that the peak temperature is located within the magneto-dielectric MF500F-112, where the substrate losses are the most significant. A report of the simulated maximum temperature generated within the MF500F-112 substrates for different power densities across the absorption spectral band is summarized in Table V. It can be seen that the temperature increases with the power density and is virtually the same across the operation band. The transient simulation is also performed on the multilayer absorber. The 3D temperature distribution throughout the absorber is obtained within a one-hour time frame for various power densities at the center frequency as shown in Fig. 15. The initial temperature of the absorber is set to the room temperature (T_0 = 20 ºC). The transient simulated results show that the temperature within the absorber increases with time and converges to the steady state after one hour. The plot in Fig. 16 (maximum temperature versus time) is provided to illustrate the trend of the temperature increase over time within the MF500F magneto-dielectrics. It is observed that the temperature rises quickly for higher incident power densities. Based on the data projected, the maximum average power density the absorber can tolerate at OFF state for an incident CW is about S_A = 10 kW/m^2.

However, the question remains if the average power handling capability of the absorber obtained at OFF state is still valid for all the plasma tuning states. Theoretically, at ON state when the plasma frequency ω_p increases, its inductance value ($L_P = \omega_P^{-2} C_0^{-1}$) as modeled in [14] decreases, as well as its resistance value ($R_P = \nu L_P$). The change in the plasma resistance can affect the temperature generated from energy dissipated through Joule effect heating. Therefore, it is possible that the radiation of the plasma electron temperature via heat transfer can also alter the temperature distribution of the absorber under high power continuous wave excitation at ON state. To demonstrate this ambiguity, even though the transition between tuning states are not abrupt, the distribution of the volume power loss density within the multilayer absorber is investigated for the discrete tuning states of the plasma shown in Fig. 6(b). The description of these tuning states is illustrated in Table VI, where each plasma state is associated with their respective plasma frequency and absorption center frequency.

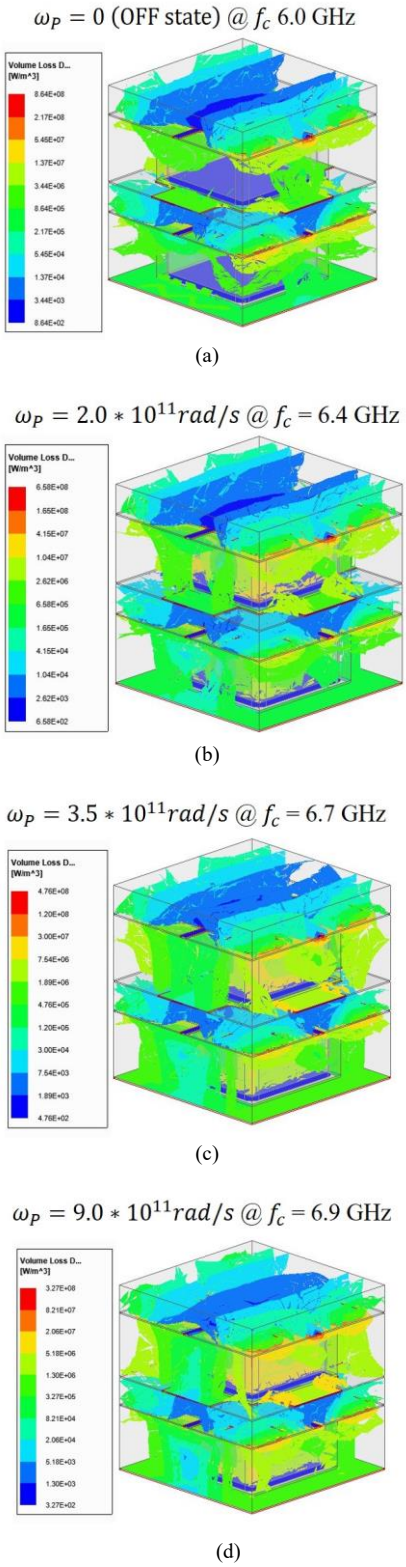

Fig. 17. Simulated volume power loss density in a unit cell of the multilayer absorber exposed to an incident power of 1W. (a) OFF state; (b) ON State #1; (c) ON State #2; (d) ON State #3.

When the absorber unit cell is illuminated with an incident power of 1W, simulated results in Fig. 17 predict that the dissipated power is localized in the substrates, with the magneto-dielectrics serving as the main contributor to the

This article has been accepted for publication in a future issue of this journal, but has not been fully edited. Content may change prior to final publication. Citation information: DOI 10.1109/TAP.2021.3070088, IEEE Transactions on Antennas and Propagation

losses. As predicted, for different tuning states of the plasma at their specific center frequency, the volume loss density value has proportionally decreased with the increase of the plasma frequency. We further investigate the transient state thermal analysis of the multilayer absorber exposed to the tolerated incident power density obtained previously at OFF state (S_A =10 kW/m^2) for all the tuning states of the plasma described in Table VI. Simulated results (see Fig. 18) predict that lower temperatures are generated within the MF500F-112 substrates at ON state cases with respect to the OFF-state case. Based on this study, the incident power density S_A =10 kW/m^2 is in fact the average maximum power handling capability of the design for all plasma states.

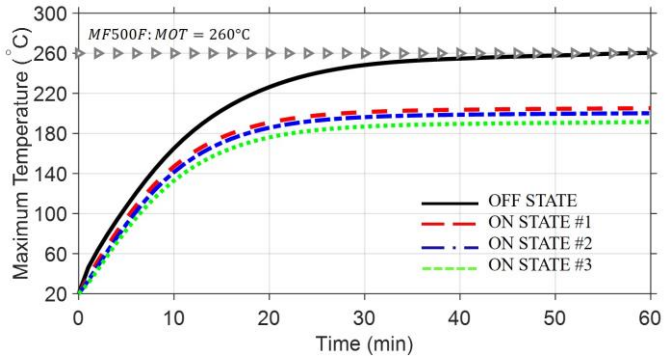

Fig. 18. Time-variant simulated peak temperature plot at various plasma states throughout the MF500F-112 substrates when exposed to S_A =10 kW/m^2 power density with incident plane EM wave at their specific absorption center frequency.

C. Experimental results of the temperature distribution on the top surface of the absorber

Testing the power handling capability of specific microwave components requires technical safety measures. All the test instruments need to be rated for the measurement environment. Safety practices recommended by IEEE standards on high power testing should be adopted. The measurement techniques of microwaves components are implemented based on the specific type of device under test (DUT). For example, when testing the power handling of a microwave filter, the input of the DUT can be driven with a coax connection and the output terminated using a high-power load. Radiated susceptibility measurement of antennas is often performed in a semi-anechoic chamber. However, all these test procedures require the use of a high-power source. To validate the thermal numerical results of the multilayer tunable plasma-based absorber, a 40 dB traveling-wave tube (TWT) amplifier from Hughes (Model#: 1177H13F000) operating in the S/C-band (3 GHz to 8 GHz) is used to generate a high power microwave. Since the power handling limit of the absorber is related to the thermal effect, the temperature of the absorbing material under RF fields is measured using a thermal imaging infrared camera (FLIR E6). This IR camera has the capability to detect object temperatures ranging from -20 ºC to 250 ºC with ±2% reading accuracy. As a safety precaution, the thermal analysis tests are performed with relatively moderate far field power densities. Although the incident power level might not test the design to its limits, it is sufficient enough to cause heat generation that can be measured using the IR camera. An illustrative sketch of the test setup is shown in Fig. 19(a). Prior to the experiment, a sinusoidal wave produced by Keysight's E8257D PSG RF analog signal generator (2500 kHz to 20 GHz) is amplified by the TWT power amplifier and the output is monitored using the E4418B EPM series power meter. Thus, by placing the DUT at the far-field (0.5 m) from the PE9887-11 broadband horn antenna, the incident power density is evaluated using the equation:

$$S = \frac{P_t G_t}{4\pi R^2} \tag{5}$$

where P_t is the transmitted power, G_t = 12.6 is the gain of the transmit horn antenna, and R is the distance from the horn antenna to the center of the top surface of the DUT. The measured thermal map is obtained at two different power densities (S = 0.2 and 0.3 kW/m^2). A photograph of the test measurement is shown in Fig. 19(b). Since only the top surface

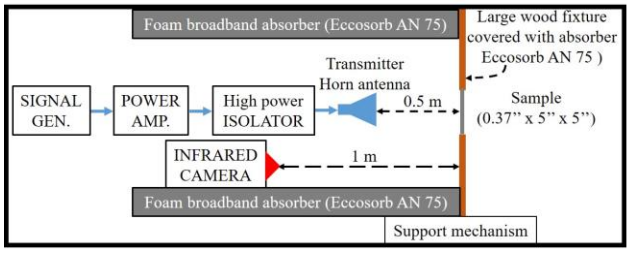

(a)

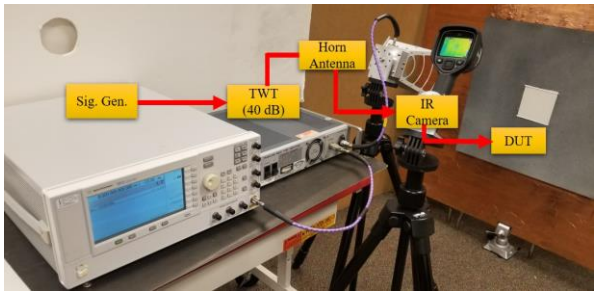

(b)

Fig. 19. (a) Sketch and (b) photograph of the free space test setup.

of the absorber is visible to the FLIR E6 IR camera, the temperature distribution on the top surface of the absorber is measured and compared to the numerical results. The numerical analysis of the thermal transient state of the absorber upon an incident RF power density at 6 GHz is performed. The simulated temperature distributions obtained on the top surface of the absorber at OFF state are shown in Fig. 20(a). In order to accurately measure the radiated temperature on top of the absorber, the IR camera is properly calibrated, the emissivity is set to 0.9 and the distance between the object and camera is set to 1.0 m. Images obtained from the IR camera are depicted in Fig. 20(b). It shown that the top surface of the absorber becomes hotter with different time frames. The qualitative aspect of the simulated temperature profile does not exactly correspond to the measured temperature map obtained of the top surface of the multilayer absorber. Several parameters such as the color

This article has been accepted for publication in a future issue of this journal, but has not been fully edited. Content may change prior to final publication. Citation information: DOI 10.1109/TAP.2021.3070088, IEEE Transactions on Antennas and Propagation

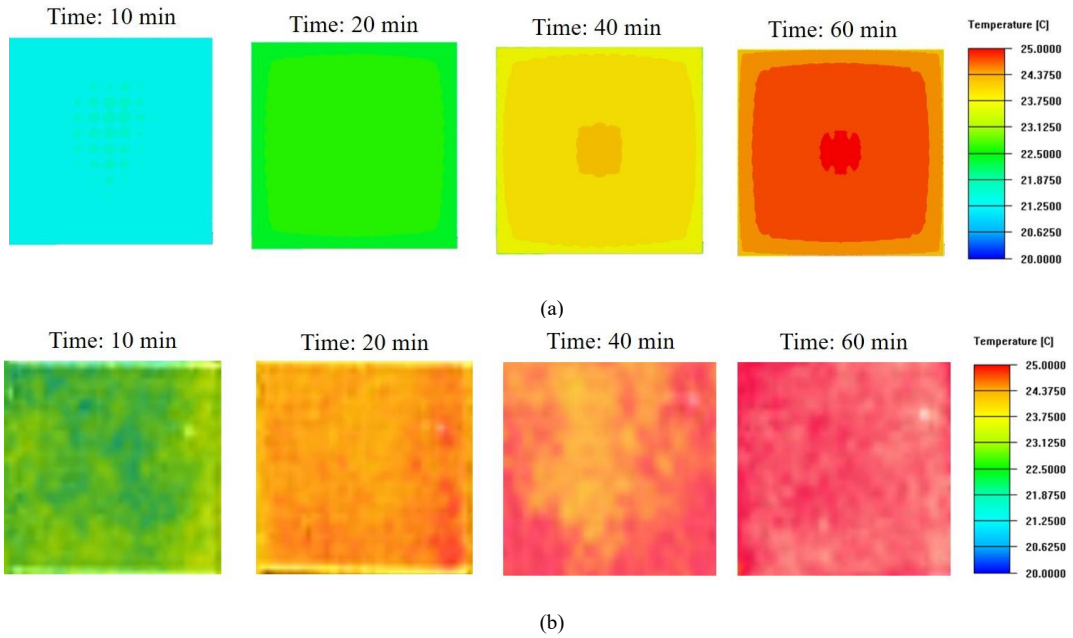

Fig. 20. Transient state temperature map observed at the top surface of the multilayer absorber (at OFF state) exposed to a power density S = 0.2 kW/m^2. (a) Simulated results for incident plane EM wave at f_0 = 6 GHz; (b) Measured results for incident plane EM wave at f_0 = 6.1 GHz.

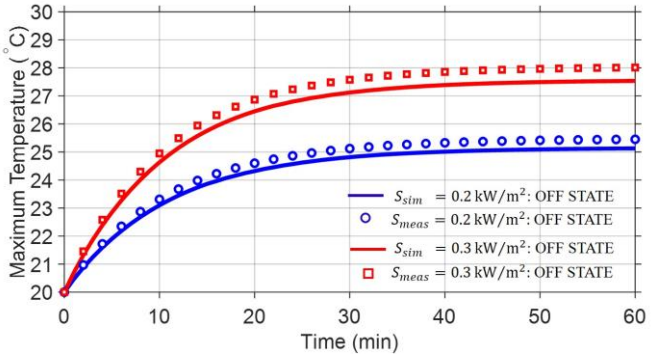

Fig. 21. Simulated/measured time-variant temperature plots obtained at the center of the top surface of the absorber at OFF state illustrated for various power densities.

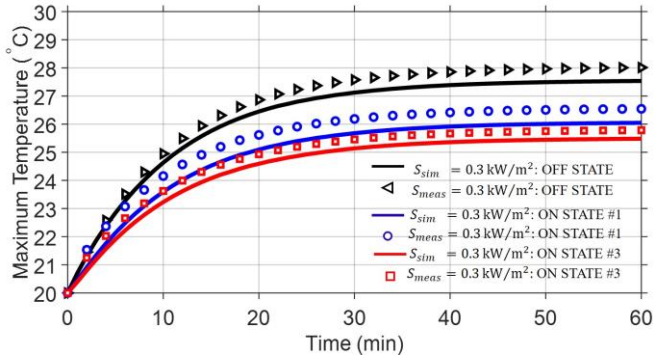

Fig. 22. Simulated/measured time-variant temperature plots obtained at the center of the top surface of the absorber illustrated for various plasma states with incident power density set to 0.3 kW/m^2.

visualization used in the simulation of the design model, the lighting in the test room, the air flow in the room or the position of the IR camera surely influence the results. However, the measured temperature obtained at the center of the top surface of the multilayer absorber accurately validates its numerical counterpart as observed in Fig. 21 for various incident power densities. Furthermore, by fixing the incident power density to 0.3 kW/m^2, the transient measured temperature at the center of the top surface is obtained for the discrete tuning states of the plasma (described in Table VI). The measured results agree well with their numerical counterpart results shown in Fig. 22.

IV. Conclusion

A compact multilayer tunable absorber based on lossy magneto-dielectric substrates embedded with discrete plasma-shells is proposed in this paper. The discrete plasma-shells located on different layers of the structure allow independent control of each resonant frequency. The techniques employed in the proposed design lend much freedom to customize both functional and physical characteristics of the absorber. This thickness customizable compact multilayer absorber is tuned in real time to provide a multifunctional response on demand for a dynamic use of the EM spectrum. Due to the vulnerability of microwave absorber when exposed to high power microwave/electromagnetic pulse (HPM/EMP), the power handling capability of our proposed multilayer absorber is studied. Notably, we investigate the physical effect of high peak and average power, which present severe challenges in a harsh electromagnetic environment. Coupled physical phenomena between both RF and thermal simulation provides rigorous multiphysics simulated results, thus predicts very well the thermal issues for high-power applications. High power

analysis of microwave components is very crucial in a sense that selected materials can be rightfully chosen in the early stages of design in order to avoid failure of the final product for specific applications and assure a safe operating in harsh environments. Per se, multiphysics analysis can result in optimized design techniques to reduce susceptibility of microwave components to fail under high power excitation. Custom design techniques such as the use of hollow pyramidal and honeycomb lossy materials, integration of a cooling system within the design, and the use of high temperature materials can increase the power handling capability. The outcomes of our research will lead to a new class of reconfigurable, high performance, high-order microwave absorbers for stable communication links from high power interference.

REFERENCES

[1] J. Jin and S. Yan, "Multiphysics modeling in electromagnetics: Technical challenges and potential solutions," *IEEE Antennas Propag. Mag.*, vol. 61, no. 2, pp. 14–26, Apr. 2019.

[2] X. Sun, M. Cheng, S. Zhu, and J. Zhang, "Coupled electromagnetic-thermal-mechanical analysis for accurate prediction of dual-mechanical-port machine performance," *IEEE Trans. Ind. Appl.*, vol. 48, no. 6, pp. 2240–2248, Nov. 2012.

[3] D. C. Schleher, *Introduction to Electronic Warfare*. Dedham, MA, USA: Artech House, 1986.

[4] A. E. Spezio, "Electronic warfare systems," *IEEE Trans. Microw. Theory Techn.*, vol. 50, no. 3, pp. 633–644, Mar. 2002.

[5] D. C. Schleher, *Electronic Warfare in the Information Age*. Norwood, MA, USA: Artech House, 1999.

[6] G. H.-H. Sung, K. W. Sowerby, M. J. Neve, and A. G. Williamson, "A frequency-selective wall for interference reduction in wireless indoor environments," *IEEE Antennas Propag. Mag.*, vol. 48, no. 5, pp. 29–37, Oct. 2006.

[7] S. Scott, C. D. Nordquist, J. Custer, D. Leonhardt, T. S. Jordan, and C. T. Rodenbeck, "Band-selective interferer rejection for cognitive receiver protection," in *IEEE MTT-S Int. Microw. Symp. Dig.*, Jun. 2013, pp. 1–4

[8] L. W. Cross, M. J. Almalkawi, and V. K. Devabhaktuni, "Theory and demonstration of narrowband bent hairpin filters integrated with AC-coupled plasma limiter elements," *IEEE Trans. Electromagn. Compat.*, vol. 55, no. 6, pp. 1100–1106, Dec. 2013.

[9] K. Payne, J. H. Choi, E. F. Peters, D. K. Wedding, C. A. Wedding, and J. Brunett, "Second-order plasma enabled tunable low-profile frequency selective surface based on coupling inter-layer," in *Proc. 46th Eur. Microw. Conf.*, Oct. 2016, pp. 309–312.

[10] E. Rocas et al., "Superconducting multiplexer filter bank for a frequency-selective power limiter," *IEEE Trans. Appl. Supercond.*, vol. 21, no. 3, pp. 542–546, Jun. 2011.

[11] P. Phudpong and I. C. Hunter, "Frequency-selective limiters using nonlinear bandstop filters," *IEEE Trans. Microw. Theory Techn.*, vol. 57, no. 1, pp. 157–164, Jan. 2009.

[12] K. Payne, K. Xu, J. H. Choi, and J. K. Lee, "Plasma enabled adaptive absorber for high power microwave applications," *IEEE Trans. Plasma Sci.,* vol.46 , no. 4, pp. 934–942, Apr. 2018.

[13] K. Payne, J. K. Lee, K. Xu, and J. H. Choi, "Low-profile plasma-based tunable absorber," in *Proc. IEEE Antennas Propag. Soc. Int. Symp. (APSURSI)*, Jul. 2018, pp. 2065-2066.

[14] K. Payne, K. Xu, J. H. Choi, and J. K. Lee, "Electrically tunable microwave absorber based on discrete plasma-shells," *IEEE Trans. Antennas Propag.,* vol. 67, no. 10, pp. 6523–6531, Oct. 2019.

[15] S. Sciancalepore and R. Di Pietro, "Bittransfer: mitigating reactive jamming in electronic warfare scenarios," *IEEE Access*, vol. 7, pp. 156 175–156 190, 2019.

[16] B. Bai, Y. Liu, L. Song, X. Li, Y. Ding, and X. Zhang, "Passive radar jamming: A novel method using time-varying plasma," *IEEE Access*, vol. 7, pp. 120 082–120 088, 2019.

[17] E. Al-Shaer, J. Wei, K. W. Hamlen, and C. Wang, "Deception-enhanced threat sensing for resilient intrusion detection," in *Auton. Cyber Deception*, Springer, 2019, pp. 147–165.

[18] C. E. Baum, "From the electromagnetic pulse to high-power electromagnetics," *Proc. IEEE*, vol. 80, no. 6, pp. 789–817, Jun. 1992.

[19] S.-H. Min, O. Kwon, M. Sattorov, H. Jung, I.-K. Baek, S. Kim, J.-Y. Jeong, J. Jang, D.Hong, R. Bhattacharya, R. K. Barik, A. Bera, S. Park, J. Ahn, S. H. Lee, Y. J. Yoon, and G.-S. Park, "Effects on electronics exposed to high-power microwaves on the basis of a relativistic backward-wave oscillator operating on the X-band," *J. Electromagn. Waves Appl.*, vol. 31, no. 17, pp. 1875–1901, 2017.

[20] E. Van Keuren and J. Knighten, "Implications of the high-power microwave weapon threat in electronic system design," in *IEEE 1991 Int. Symp. Electromagn. Compat.*, Jul. 1991, pp. 370–371.

[21] C. Wilson, "High altitude electromagnetic pulse (HEMP) and high power microwave (HPM) devices: Threat assessments", Congressional Research Service, Washington, DC, USA, Rep. ADA529982, Jul. 21, 2008.

[22] A. Neuber, G. F. Edmiston, J. T. Krile, H. Krompholz, J. C. Dickens, and M. Kristiansen, "Interface breakdown during high-power microwave transmission," *IEEE Trans. Magn.*, vol. 43, no. 1, pp. 496–500, Jan. 2007.

[23] C. M. Sabliov, D. A. Salvi, and D. Boldor, "High frequency electromagnetism, heat transfer and fluid flow coupling in ANSYS multiphysics," *J. Microw. Power Electromagn. Energy*, vol. 41, no. 4, pp. 5–17, 2006.

[24] D. Salvi, D. Boldor, J. Ortego, G. M. Aita, and C. M. Sabliov, "Numerical modeling of continuous flow microwave heating: A critical comparison of COMSOL and ANSYS," *J. Microw. Power Electromagn. Energy*, vol. 44, no. 4, pp. 187–197, 2010.

[25] B. A. Munk, *Frequency Selective Surfaces: Theory and Design*. New York, NY, USA: Wiley, 2000.

[26] E. F. Knott, J. F. Shaeffer, and M. T. Tuley, *Radar Cross Section*. Dedham, MA, USA: Artech House, 1985.

[27] L. J. Du Toit, "The design of Jauman absorbers," *IEEE Antennas Propag. Mag.*, vol. 36, no. 6, pp. 17–25, Dec. 1994.

[28] W. Dallenbach, and W. Kleinsteuber, "Reflection and absorption of decimetre-waves by plane dielectric layers," *Hochfreq. U Elektroak*, vol 51, pp. 152–156, 1938.

[29] Y. Shang, Z. Shen, and S. Xiao, "On the design of single-layer circuit analog absorber using double-square-loop array," *IEEE Trans. Antennas Propag.*, vol. 61, no. 12, pp. 6022–6029, Dec. 2013.

[30] N. Engheta, "Thin absorbing screens using metamaterial surfaces," in *IEEE Antennas Propag. Soc. Int. Symp.*, Jun. 2002, vol. 2, pp. 392–395.

[31] F. Costa, A. Monorchio, and G. Manara, "Analysis and design of ultra-thin electromagnetic absorbers comprising resistively loaded high impedance surfaces," *IEEE Trans. Antennas Propag*., vol. 58, no. 5, pp. 1551–1558, May 2010.

[32] A. Kazem Zadeh and A. Karlsson, "Capacitive circuit method for fast and efficient design of wideband radar absorbers," *IEEE Trans. Antennas Propag.*, vol. 57, no. 8, pp. 2307–2314, Aug. 2009.

[33] W. Tang, G. Goussetis, H. Legay, and N. J. G. Fonseca, "Efficient synthesis of low-profile angularly-stable and polarization-independent frequency-selective absorbers with a reflection band," *IEEE Trans. Antennas Propag.*, vol. 63, no. 2, pp. 621–629, Feb. 2015.

[34] K. N. Rozanov, "Ultimate thickness to bandwidth ratio of radar absorbers," *IEEE Trans. Antennas Propag*., vol. 48, no. 8, pp. 1230–1234, Aug. 2000.

[35] A. Tennant and B. Chambers, "A single-layer tuneable microwave absorber using an active FSS," *IEEE Microw. Wireless Compon. Lett.*, vol. 14, no. 1, pp. 46–47, Jan. 2004.

[36] J. Zhao, Q. Cheng, J. Chen, M. Q. Qi, W. X. Jiang, and T. J. Cui, "A tunable metamaterial absorber using varactor diodes," *New J. Phys.*, vol. 15, no. 4, Apr. 2013, Art. no. 43049.

[37] T. Nesimoglu and C. Sabah, "A frequency tunable metamaterial resonator using varactor diodes," in *Proc. 16th Medit. Microw. Symp. (MMS)*, Nov. 2016, pp. 1–4.

[38] C. Mias and J. H. Yap, "A varactor-tunable high impedance surface with a resistive-lumped-element biasing grid," *IEEE Trans. Antennas Propag.*, vol. 55, no. 7, pp. 1955–1962, Jul. 2007.

[39] V. F. Fusco, R. Cahill, W. Hu, and S. Simms, "Ultra-thin tunable microwave absorber using liquid crystals," *Electron. Lett.,* vol. 44, no. 1, pp. 37–38, Jan. 2008.

[40] B. Xu, C. Gu, Z. Li, L. Liu, and Z. Niu, "A novel absorber with tunable bandwidth based on graphene," *IEEE Antennas Wireless Propag. Lett.*, vol. 13, pp. 822–825, 2014.

[41] Y. Zhang, Y. Feng, B. Zhu, J. Zhao, and T. Jiang, "Graphene based tunable metamaterial absorber and polarization modulation in terahertz frequency," Opt. Express, vol. 22, no. 19, pp. 22743–22752, 2014.

[42] K. Payne, J. K. Lee, K. Xu, and J. H. Choi, "Higher order plasma-based tunable absorber using magneto-dielectric substrates," in *Proc. IEEE Antennas Propag. Soc. Int. Symp. (APSURSI),* Jul. 2019, pp. 2027–2028.

[43] K. Payne, K. Xu, and J. H. Choi "Generalized synthesized technique for the design of thickness customizable high-order bandpass frequency selective surface," *IEEE Trans. Microw. Theory Techn*., vol. 66, no. 11, pp. 4783–4793, Nov. 2018.
[44] M. A. Lieberman and A. J. Lichtenberg, *Principles of Plasma Discharges and Materials Processing*. Hoboken, NJ, USA: Wiley, 2005.
[45] P. Baille, J.-S. Chang, A. Claude, R. M. Hobson, G. L. Ogram, and A. W. Yau, "Effective collision frequency of electrons in noble gases," *J. Phys. B, Atomic Mol. Phys.*, vol. 41, no. 9, pp. 1485–1495, 1981.
[46] M. Li and N. Behdad, "Frequency selective surfaces for pulsed high-power microwave applications," *IEEE Trans. Antennas Propag.*, vol. 61, no. 2, pp. 677–687, Feb. 2013.
[47] D. Fitzpatrick, "Chapter 15 - temperature analysis," in *Analog Design and Simulation Using OrCAD Capture and PSpice*, 2nd ed. Cambridge, MA, USA: Newnes, 2018, pp. 209–216.

Komlan Payne (S'13) received the B.S. (*summa cum laude*) and the Ph.D. degrees in electrical engineering from Syracuse University, Syracuse, NY, USA, in 2014 and 2020 respectively.

From 2014 to 2020, he has been a Research Assistant with the Microwave Laboratory, Department of Electrical Engineering and Computer Science, Syracuse University. His graduate research interests include antennas miniaturization, RF/microwave circuits, and frequency-selective surfaces and absorbers.

Currently, he is a Postdoctoral Associate with the Department of Biomedical Engineering, University at Buffalo, The State University of New York, Buffalo, NY, USA. His current research interests include the development of advanced Microwave Resonance RF detectors and transmitters for human diagnosis, fast MR imaging methodologies (e.g. parallel imaging algorithm, compressed sensing, machine learning), design and construction of innovative RF coils and coil arrays and its in vivo applications.

Kevin Xu (S'14) received the B.S. and M.S. degrees in electrical engineering from Syracuse University, Syracuse, NY, USA, in 2016 and 2017, respectively. He is currently pursuing the Ph.D. degree at the University at Buffalo, The State University of New York, Buffalo, NY, USA.

His current research interests include electromagnetic absorbers, frequency selective surfaces, and retrodirective arrays. Mr. Xu was a recipient of the Anaren Gerst-Hair Graduate Studies Fellowship Award.

Jun H. Choi (S'12–M'14) received the B.S. degree in electrical engineering from the University of California, Irvine, CA, USA, in 2003, and the M.S. and Ph.D. degrees in electrical engineering from the University of California at Los Angeles, Los Angeles, CA, USA, in 2006 and 2014, respectively.

Currently, he is an Assistant Professor with the Department of Electrical Engineering, University at Buffalo, The State University of New York, Buffalo, NY, USA. From 2017 to 2019, he was an Assistant Research Professor, and from 2014 to 2017, he was an Assistant Professor with the Department of Electrical Engineering and Computer Science, Syracuse University, NY, USA. His current research interests include planar antennas, frequency-selective surfaces, and microwave devices based on CRLH, and metamaterial structures.

Dr. Choi was a recipient of the 2017 AFOSR Young Investigator Award.

Jay Kyoon Lee (S'80–M'85–SM'91) received the B.S. degree in electronics engineering from Seoul National University, Seoul, South Korea, in 1976 and the M.S. and Ph.D. degrees in electrical engineering from the Massachusetts Institute of Technology, Cambridge, MA, USA, in 1981 and 1985, respectively.

Since 1985, he has been with the Faculty of the Department of Electrical Engineering and Computer Science, Syracuse University, Syracuse, NY, USA. From 1987 to 1988, he was with the Naval Air Development Center, Warminster, PA, USA, where he was involved in the SAR imaging problem. In 1990, he was a Visiting Professor with the Rome Air Development Center, Rome, NY, USA. In 1993, he was with the Naval Research Laboratory, Washington, DC, USA. In 2000, he was an Invited Visiting Professor with Seoul National University. He has coauthored *Electromagnetics* (Adams & Lee, University Readers, 2012; Cognella, 2019). His current research interests include electromagnetic fields and waves, microwave remote sensing, waves in anisotropic and gyrotropic media, antennas and propagation, and microwave engineering.

Dr. Lee is a member of the American Geophysical Union and the Korean–American Scientists and Engineers Association (KSEA) in America and a fellow of the Electromagnetics Academy. He was a recipient of the Eta Kappa Nu Outstanding Undergraduate Teacher Award from Syracuse University in 1999, the IEEE Third Millennium Medal in 2000, the College Educator of the Year Award from the Technology Alliance of Central New York in 2002, and the IEEE Region 1 Awards in 2003 and 2017. He has been on the International Editorial Board of the *Progress in Electromagnetics Research* since 1993. He has served as the President for the Upstate New York Chapter of the KSEA from 1990 to 1991, as the Chair for the IEEE Syracuse Section from 1995 to 1996, as the Student Activities Committee Chair for the IEEE Region 1 from 1996 to 2000, and as the Faculty Advisor for the IEEE Student Branch of Syracuse University from 1996 to 2018.